SPE-190155-MS

Upscaling Laboratory Result of Surfactant-Assisted Spontaneous Imbibition to the Field Scale through Scaling Group Analysis, Numerical Simulation, and Discrete Fracture Network Model

Fan Zhang, I. W. R. Saputra, Geng Niu, and Imad A. Adel, Texas A&M University; Liang Xu, Halliburton; David S. Schechter, Texas A&M University

This paper was prepared for presentation at the SPE Improved Oil Recovery Conference held in Tulsa, Oklahoma, USA, 14-18 April 2018.

Abstract

Field experience along with laboratory evidence of spontaneous imbibition via the addition of surfactants into the completion fluid is widely believed to improve the IP and ultimate oil recovery from unconventional liquid reservoirs (ULR). During fracture treatment with surface active additives, surfactant molecules interact with the rock surface to enhance oil recovery through wettability alteration combined with interfacial tension (IFT) reduction. The change in capillary force as the wettability is altered by the surfactant leads to oil being expelled as water imbibes into the pore space. Several laboratory studies have been conducted to observe the effectiveness of surfactants on various shale plays during the spontaneous imbibition process, but there is an insufficient understanding of the physical mechanisms that allow scaling the lab results to field dimensions.

In this manuscript, we review and evaluate dimensionless, analytical scaling groups to correlate laboratory spontaneous imbibition data in order to predict oil recovery at the field scale in ULR. In addition, capillary pressure curves are generated from imbibition rate theory originally developed by Mattax and Kyte (1962).The original scaling analysis was intended for understanding the rate of matrix-fracture transfer for a rising water level in a fracture-matrix system with variable matrix block sizes. Although contact angle and interfacial tension (IFT) are natural terms in scaling theory, virtually no work has been performed investigating these two properties. To that end, we present scaling analysis combined with numerical simulation to derive relative permeability curves, which will be imported into a discrete fracture network (DFN) model. We can then compare analytical scaling methods with conventional dual porosity concepts and then progressed to more sophisticated Discrete Fracture Network concepts. The ultimate goal is to develop more accurate predictive methods of the field-scale impact due to the addition of surfactants in the completion fluid.

Correlated experimental workflows were developed to achieve the aforementioned objectives including contact angle (CA) and IFT at reservoir temperature. In addition, oil recovery of spontaneous imbibition experiments was recorded with time to evaluate the performance of different surfactants. Capillary pressure-based scaling is developed by modifying previously available scaling models based on available surfactant-related properties measured in the laboratory. To ensure representability of the scaling method; contact angle, interfacial tension, and ultimately spontaneous imbibition experiments were performed on field-retrieved samples and used as a base for developing a new scaling analysis by considering dimensionless recovery and time. Based on the capillary pressure curves obtained from the scaling model, relative permeability is approximated through a history matching procedure on core-scale numerical models. CT-Scan technology is used to build the numerical core plug model in order to preserve the heterogeneity of the unconventional core plugs and visualize the process of water imbibition in the core plugs. Time-lapse saturation changes are recorded using the CT scanner to visualize penetration of the aqueous phase into oil-saturated core samples. The capillary and relative permeability curves can then be used on DFN realizations to test cases with or without surfactant. The results of spontaneous imbibition showed that surfactant solutions had a higher oil recovery due to wettability alteration combined with IFT reduction. Our upscaling results indicate that all three methods can be used to scale laboratory results to the field. When compared to a well without surfactant additives, the optimum 3-year cumulative oil production of well that is treated with surfactant can increase by more than 20%.

Introduction

Unconventional liquid reservoirs (ULR) have played a significant role in domestic oil production for almost a decade and has led the United States to become one of the largest oil producers in the world (Adel et al. 2016). The recent success in developing these reservoirs is driven by multistage hydraulic fracturing technology, a necessity due to the ultralow permeability that characterizes ULR. Fracture networks generated from the multistage hydraulic fracturing completions interacting with naturally occurring fractures provides crucial flow paths for liquids to flow from the reservoir. Multiple laboratory studies have shown that in comparison to the base case of water without surfactant, the presence of surfactant increases both the rate of production and ultimate recovery of oil (Alvarez et al. 2014). With numerous variables determining the efficacy of a multistage hydraulic fracturing treatment, optimization of surface active agents (molecular type, volume, concentration…etc.). Provides an excellent opportunity to improve performance in old and new wells across vast acreage characteristic of these resource plays.

Surfactant molecules act as a bridge between the two immiscible phases present in the pore system, oil and water, with the two segments of the molecule, known as head and tail, possess different affinity to the aqueous and oleic phases. The head of the surfactant molecule is hydrophilic, having a higher affinity towards the aqueous phase, and the tail portion of the surfactant molecule which is hydrophobic, thus having a higher affinity towards crude oil molecule. Partitioning of the head group in the aqueous phase and the tail group in the oleic phase primarily results in lowering of the oil-water interfacial tension. In addition, certain surface active agents result in alteration of wettability from a natural oil-wet surface observed in all resource reservoirs investigated to water-wet. The degree and magnitude of IFT and wettability alteration are subject to intense scrutiny to understand how to design the optimum system for each different application. The capillary force acts as the driving force for spontaneous imbibition observed in lab experiments as oil is expelled from the larger pore spaces as water imbibes into, the smaller pores(Alvarez and Schechter 2015). Wettability and interfacial tension are two out of three variables that control the magnitude of capillary force as a consequence of the Young-Laplace equation.

A complete and systematic gathering of experimental data to evaluate each surfactant-related property is already available in the literature (Alvarez and Schechter 2017). Since the experimental part of this study is focused on supplying required data for the upscaling process, measurements listed in the referenced literature in which we only examine the measurements related to upscaling. Interfacial tension of oil and water is an essential variable in the surfactant-assisted spontaneous imbibition, acting as the driving force once the wettability is altered. The pendant drop method is used to measure the interfacial tension due to the accuracy of this method in the range of IFT value encountered with the surfactants used in our studies (0.1

– 30 mN/m). The measurement of the contact angle is the preferential method to determine the wettability of the rock. Since injection into the core from resource plays is not possible, saturation, re-saturation and classic techniques such as the Amott or USBM techniques are simply not feasible. Thus static contact angle on reservoir surfaces aged in crude oil has been extensively reported as the quantitative determination of wettability.

Scaling models for spontaneous imbibition have been studied since the 1960's, yet there are very limited scaling studies reported for unconventional reservoirs. Mattax and Kyte (1962) initially proposed a dimensionless group that can be used to scale imbibition. Ma et al. (1995) modified the scaling model defined in Eq. 1 by considering the geometry and shape of rock samples, boundary conditions, and oil-water viscosity ratio. In addition, the characteristic length factor (Lc) is defined by Ma's model which is commonly used in the other scaling models. This length factor can be described as fracture spacing in naturally fractured reservoirs.

$$t_D = t\sqrt{\frac{k}{\emptyset}}\,\frac{\sigma}{\sqrt{\mu_o \mu_w}}\,\frac{1}{{L_c}^2} \tag{1}$$

Where t is the actual time of imbibition, k and ϕ are permeability and porosity respectively, σ is IFT, and μ_w is water viscosity. Characteristic length factor for different flow regimes and laboratory setups for imbibition experiments are found in the publication from Fischer et al. (2008). However, the scaling model presented in Eq. 1 does not consider the wettability effect without the presence of contact angle. Gupta and Civan (1994) introduced the wettability term into Ma's model via the contact angle. The new scaling group is shown in Eq. 2, where the contact angle represents wettability of the rock surface. In this study, we focus on wettability alteration and moderate IFT reduction to improve oil recovery in ULR. The wettability is the focus in our scaling group analysis. Thus, we select Eq. 2 as the scaling model to analyze spontaneous imbibition and upscale the laboratory data to the field.

$$t_D = t\sqrt{\frac{k}{\emptyset}}\,\frac{\sigma\cos\theta}{\sqrt{\mu_o \mu_w}}\,\frac{1}{{L_c}^2} \tag{2}$$

Li and Horne (2002) defined a general scaling approach for spontaneous imbibition in both co-current and countercurrent cases, which includes the use of wetting and non-wetting phase relative permeability. The equation for dimensionless time is shown in Eq. 3, where c is a constant value for the ratio of the gravity force to the capillary force; k_{re}^* is the relative permeability pseudofunction of the two phases at S_{wf}; P_c^* is capillary pressure at S_{wf}; S_{wi} is the initial water saturation, and $\mu_e$is effective viscosity of the two phases. This scaling model can be used in almost any conventional rock systems (Adel et al. 2018). Due to the ultralow permeability and low porosity in ULR, it is very difficult to measure the capillary pressure and relative permeability for the rock-fluid interaction, therefore this scaling approach is not suitable for unconventional rocks.

$$t_D = c^2\,\frac{k k_{re}^*}{\phi}\,\frac{P_c^*}{\mu_e}\,\frac{S_{wf}-S_{wi}}{L_c^2}\,t \tag{3}$$

Upscaling surfactant-assisted spontaneous imbibition laboratory results to the field is a relatively new subject with few studies reported in the literature. Wang et al. (2016) used an analytical method to scale experimental laboratory data from Bakken to the field. The authors assumed the dimensionless time at which half of the oil has been produced in the rock has the same value in the lab experiments as in the field. In our study, we assume the dimensionless time is the same value for the lab scale and the field scale. Thus a field production rate can be predicted analytically. In addition, a dual porosity simulation model and a DFN model are also developed in order to upscale the laboratory results to the field.

The approach of discrete fracture network (DFN) is widely used to study the propagation of hydraulic fractures (Parsegov et al. 2018), and production related behavior of the fractured reservoir (Du et al. 2017; Sun and Schechter 2017; Sun and Schechter 2015). DFN represents the high-permeability paths generated when the hydraulic fracture is interacting with a natural fracture that is most certainly present pervasively in the reservoir rock. The unstructured mesh utilized could accurately capture the complex fracture geometry with low computation requirements, compared to a structured grid. The complexity of a DFN such as extensive fracture clustering, non-orthogonal, and low-angle fracture intersections can be handled, thus vastly improving the sugar cube model requiring empirical transfer functions in dual-porosity reservoirs. Another advantage of this explicit approach is to minimize the grid orientation effect inside fractures and distribute the aperture of fractures as observed in naturally occurring fractures.

The purpose of this study is to develop reliable methods for upscaling laboratory results to the field, by evaluating the effectiveness of surfactant to completion fluid in enhancing oil recovery in ULR. First, CA and IFT measurements are performed to study the capability of surfactants in wettability alteration and IFT reduction. Then, spontaneous imbibition experiments are conducted to analyze the impact of surfactants on ultimate oil recovery along with time-lapse CT scan technology in order to visualize water penetration into the core and to generate the core porosity model for history match simulation of spontaneous imbibition. Next, capillary pressure and relative permeability curves of ULR core samples are obtained by scaling group analysis and history matching spontaneous imbibition results, respectively. Finally, laboratory results are upscaled by scaling group analysis, dual porosity models, and DFN models to estimate field production and compare the upscaling results by all three methods.

Methodology

Three upscaling methods used and compared in this study to upscale the laboratory study of Surfactant-Assisted Spontaneous Imbibition (SASI) method, analytical, dual porosity numerical simulation, and DFN numerical models, are described in this section. Moreover, an overview of all necessary laboratory experimental work to supply the required data for the upscaling process is also provided, which consists of interfacial tension, contact angle, and spontaneous imbibition experiment.

Experimental Procedure

Rock samples used in this study are retrieved from sidewall core of a well in the liquid-rich part of Eagle Ford with the oil produced from the corresponding formation. Core plugs dimensions are 1-inch in diameter with length ranging from 2 to 2.5 inch. Porosity measurement performed on helium porosimeter gives the porosity value of 8.7% and permeability to air of 200 nD. X-Ray diffraction shows that the rocks are dominated by carbonate minerals such as calcite, which comprises 40% of the total composition compared to quartz which makes 17% of the total composition. The crude oil density is 44.9 lb/ft^3 measured at the reservoir temperature of 180°F.

Three different fluid system are tested in this study: DW, Surf1, and Surf2. Fluid system DW is a base case of water without surfactant and fluid system Surf1 and Surf2 are two different surfactant solutions with the concentration of 2 gpt, equaling to 0.2 vol%. The two surfactants tested have different charges at the head group of the molecule. Surf1 is an anionic surfactant which has a negatively-charged head while Surf2 is a cationic surfactant which has a positively-charged head.

IFT is measured based on the pendant drop method utilizing a Dataphysics OCA 15 Pro device. An oil drop is dispensed upward through a needle which is submerged in the aqueous fluid system. A hi-speed camera then captures the image of the oil bubble precisely before it detaches from the needle and software is used to calculate the IFT value from the pendant drop image. The IFT value between oil and each of the three fluid systems are measured respectively and then input to the scaling group analysis to generate the capillary pressure curves. All measurements are performed at the reservoir temperature of 180°F.

Contact angle measurement is performed with the identical Dataphysics OCA 15 Pro, but set up differently in order to execute the captive bubble method. A rock sample is submersed and positioned on a surface in the fluid system to be tested. The ad oil drop is placed below the shale facing the surface of the rock. An image of the oil bubble attached to the rock surface is recorded by the hi-speed camera, and the angle of the bubble is calculated by the software. The contact angle value is incorporated into the analytical scaling group method. Similar to the interfacial tension measurement, measurements are performed at reservoir temperature of 180°F.

More detail on the procedure of contact angle and interfacial tension measurement methods used in this study are covered in the paper by Alvarez, Johannes O. et al. (2017).

For the spontaneous imbibition experiments, core plugs are aged in the crude oil for 3 months in order to restore the rock properties to its original reservoir state. More details on the aging process can be found in the reference previously mentioned. Aged core plugs are then submerged in one of the aqueous fluid systems in a modified Amott cell set up for ten days, while the amount of oil produced is recorded as it accumulates in the graduated portion at the top of the cell. In order to reduce the gravity force effect on the experiment, the core plug is positioned horizontally. The entire experimental set up is kept in an oven at reservoir temperature in order to run the experiments at the same temperature of 180°F. Spontaneous imbibition experiments are essential as it provides the oil recovery as a function of time, which is the foundation of capillary pressure curve generation from the scaling group analysis, as well as the history-match objective on the relative permeability curve generation from the history-matching process by the core-scale numerical simulation.

Capillary Pressure Obtained from Scaling Group Analysis

Oil recovery can be improved by adding surfactants to the completion fluid in ULR due to wettability alteration and IFT reduction. Wettability alteration changes the rock surface from oil wet to water wet, which allows water to be imbibed into the rock spontaneously. Spontaneous imbibition is primarily driven by capillary pressure calculated by Young-Laplace equation presented as Eq. 4, where r is pore radius.

$$P_c = \frac{2\sigma \cos\theta}{r} \tag{4}$$

Leverett (1939) defined a correlation between radius, porosity, and permeability as:

$$r \propto \sqrt{\frac{k}{\emptyset}} \tag{5}$$

Capillary force can be rewritten in term of the Leverett radius, porosity, permeability, IFT and contact angle by:

$$P_c = \frac{2\sigma \cos\theta}{\sqrt{\frac{k}{\emptyset}}} \tag{6}$$

In order to generate an imbibition capillary pressure profile for spontaneous imbibition, we defined a scaling group that considers capillary pressure and laboratory data, which is presented as Eq.7, where P_cT is our defined parameter that stands for capillary pressure multiplied by time.

$$P_c\mathrm{T} = \mathrm{t}\frac{2\sigma \cos\theta}{\sqrt{\frac{k}{\emptyset}}} \tag{7}$$

As we know the values of porosity, permeability, IFT and contact angle, we can calculate ΔP_cT based on the time used in spontaneous imbibition experiments. Since $\Delta P_c T$ can be obtained from Eq.4, ΔP_c can be calculated from Eq.8, where t_{mid} is the mean time between two recorded times in the experiments. By considering oil recovery curves obtained from spontaneous imbibition experiments, initial water saturation and ΔP_c, the capillary pressure profile can be generated.

$$\Delta P_c = \frac{\Delta P_c \mathrm{T}}{\mathrm{t_{mid}}} \tag{8}$$

Relative Permeability Obtained from History-Match on Core-Scale Numerical Model

Relative permeability, in addition to capillary pressure curve, is necessary to perform the field-scale dimensions on both the dual porosity and DFN model. The history-matching process to obtain the relative permeability data is performed by plugging in trial relative permeability curves along with capillary pressure curves obtained from the scaling group analysis to a numerical core-scale model and comparing the oil production result to that observed in the lab. This process is performed multiple times, by submitting different sets of relative permeability curves, until the best possible match of the data is achieved. Since each fluid system would have different relative permeability curves as each fluid system has different interaction between oil, rock, and water, the history-match process is performed on each of the fluid systems separately.

A numerical model of the surfactant-assisted spontaneous imbibition process done on the laboratory experiment is built in a commercial reservoir simulator which is based on the act of reaching the capillary equilibrium utilizing the capillary pressure curve obtained from the scaling group analysis. Heterogeneity is an essential aspect of modeling fluid flow in a shale sample. On the scaling group analysis, heterogeneity is implicitly included in the equation to generate the capillary pressure curve. For the numerical model, heterogeneity is imported by utilizing the CT-Scanner to create a digital rock model. By scanning each core plug used in the imbibition experiment, a 3D map of density distribution can be obtained, and this data can be converted into a digital porosity map of the core plug as explained in the work of Alvarez, J. O. et al. (2017). In order to model accurately what is observed during spontaneous imbibition, no pressure difference is applied in the simulation, meaning the capillary force is the sole cause of fluid movement in each grid block.

Upscaling Laboratory Data to Field-Scale by Dual Porosity Numerical Model

Estimation of the effect of SASI on field-scale performance with a dual porosity numerical model is performed by applying previously obtained capillary pressure and relative permeability curve on a simple mechanistic dual porosity field model. The model is built and executed on identical software used on the lab-scale model, and the only difference is that dual porosity grid configuration is used for the field-scale model. In order to save computational time, the grid model consists of only one hydraulic fracture stage with the width and length of the reservoir model being hydraulic fracture stage spacing and fracture length, respectively. Reservoir properties are not obtained from any specific part of the Eagle Ford reservoir but are generated to be as representative as possible by compiling different reservoir properties of the reservoir from various sources. The reservoir properties and grid configuration for dual porosity model are presented in Fig. 1.

Surfactants are assumed to be introduced into the reservoir as part of hydraulic fracturing fluid additives resulting in the presence of surfactant molecules initially in the fracture system. Three cases simulated are differentiated by the three different fluid systems tested in this study. The first case is the base case where capillary pressure and relative permeability curve set of the DW fluid systems is applied, whereas, for the other two cases, the curve sets of the two different surfactants used are applied. A 10-day shut-in period is assumed because this is often the approximate time scale observed in the field during shut-in between completions and tie-back to the production line. The simulation then is run for three years, the oil production and the cumulative oil recovery of three cases are compared. Final results from all cases are multiplied by 20, under the assumption that 20 hydraulic fracture stages are performed on the well.

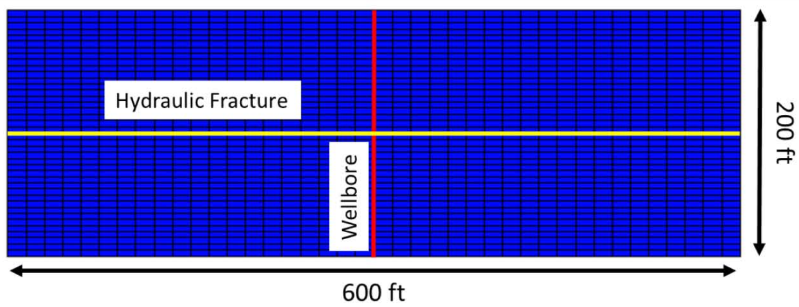

Reservoir Property	Value
Thickness (ft)	50
ϕ_m (frac.)	0.0867
ϕ_{NF} (frac.)	0.006
k_m (nd)	145
k_{NF} (nd)	300
NF Spacing (ft)	2
Sw (frac.)	0.15
Pi (psia)	9000

Figure 1—Summary of the dual porosity field-scale model.

Upscaling Laboratory Data to Field-Scale by Analytical Method

The analytical method for scaling laboratory results to the field depends on the dimensionless scaling group analysis of SASI laboratory results. For the purpose of this study, we used the scaling model presented by Gupta (Eq. 2) in order to predict the improved oil recovery by imbibition at the field scale. The scaling analysis in this paper depends on Gupta's model because all of the parameters in this model can be obtained, including both wettability and IFT terms. Capillary pressure dominates oil recovery from the rock at lab scale, but on a field scale, the main driving force for oil production is the pressure difference between the reservoir and the horizontal well. Due to an increased capillary pressure as the wettability of rock surface is altered water-wet by surfactant, the pressure difference for the oil phase between the reservoir and wellbore is increased, resulting in improved oil recovery.

Based on the Gupta's model, the dimensionless time of lab scale is governed by Eq. 2. In the meantime, the dimensionless group for the field scale model can use a similar equation that was presented in Eq. 9, where $t_{D(field)}$ is the dimensionless time in the field scale; $t_{(field)}$ is the real time at the field scale; $L_{c(field)}$ is characteristic length in the field.

$$t_{D(field)} = t_{(field)}\sqrt{\frac{k}{\emptyset}}\,\frac{\sigma\cos\theta}{\sqrt{\mu_o\mu_w}}\,\frac{1}{{L_{c(field)}}^2} \tag{9}$$

For our experimental setup, the characteristic length (Lc) for core samples fits in cylindrical scenario (all-faces-open) based on Fisher's defined Lc. The equation is presented as Eq. 10 where d is the core diameter, and l is the core length. We assumed that all characteristic length calculations in this paper follow the all-face-open scenario where:

$$L_c = \frac{ld}{2\sqrt{d^2+2l^2}} \tag{10}$$

For our lab experiments, all the sidewall core samples and oil is from the same reservoir as our field case; all the reservoir properties should be similar between the laboratory and field. Therefore, we assume that the porosity, permeability, IFT, contact angle, the viscosity of water and oil, as well as initial wettability are the same between lab and field. In order to upscale the laboratory results to field dimensions and predict the field production rate curve, we made an assumption that the dimensionless time for the laboratory experiment and in the field is the same at all times. Based on this assumption, we applied the scaling group model to both laboratory and field data in order to generate a correlation between time and characteristic length as seen in Eq. 11, which can be used to calculate the characteristic length in the field. The characteristic length in the field is then used to predict the distance that water penetrates into the reservoir matrix.

$$t_{(field)} = t_{(laboratory)}\frac{{L_{c(field)}}^2}{{L_{c(laboratory)}}^2} \tag{11}$$

By considering the surfactant type, initial water saturation, oil recovery factor obtained by spontaneous imbibition experiments, calculated field characteristic length, and fracture area, the cumulative oil production due to imbibition at a field scale can be predicted from Eq. 12, where Recovery Factor is obtained from the experimental measurements; A is total area of open fractures; S_o is initial oil saturation, and l_d is distance that water penetrates into the formation.

$$Q = Recovery\ Factor \times A \times S_o \times l_d \tag{12}$$

Since t_D values for laboratory experiments and the field are the same, the field normalized production rate curve for imbibition should have the same shape as normalized production rate curve for spontaneous imbibition experiment performed in the laboratory. The normalized production rate curve for a laboratory experiment can be calculated from the oil recovery curve which is measured in the spontaneous imbibition experiments using Eq. 13 and Eq. 14, where q is production rate, q_n is the normalized production rate, q_{max} the maximum production rate in spontaneous imbibition experiments, and t is laboratory time. By considering completion method, surfactant types, reservoir geometry, fracture surface area, and fracture geometry, oil production in the field can be predicted using Eq. 12. The field production rate can then be estimated by combining the field cumulative oil production with the normalized production rate curve.

$$q = \frac{\nabla\ Recovery\ Factor}{\nabla t} \tag{13}$$

$$q_n = \frac{q}{q_{max}} \tag{14}$$

Upscaling Laboratory Data to Field-Scale by Discrete Fracture Network Model

A DFN is generated for one stage of the hydraulic fractured well by integrating data from core observation, microseismicity and pumping schedule, described by Sun et al. (2016). Detail of the DFN is listed in Table 1. It is assumed that not all the hydraulic fluid stays in the fracture network with a considerable aperture, but a portion of the fluid invades into the matrix through pre-existing natural fractures. This results in less than 100% fluid efficiency and enhancement of matrix apparent permeability. A previous study also uses the enhanced apparent permeability to represent the effect of unpropped fracture in an unconventional reservoir (Niu et al. 2017). In this study, the matrix permeability is set as 1.5 times of that used in the dual porosity cases.

Table 1—Properties of generated DFN

Parameter Description	Set 1 (N 35 deg. E)	Set 2 (E-W)
Mean Strike	35 deg.	90 deg.
Fisher Parameter (k)	120	80
Minimum Fracture Length (lmin)	100 ft	100 ft
Maximum Fracture Length (lmax)	150 ft	200 ft
Power Law Exponent (α)	0.8	0.9
Fracture Height	50 ft	50 ft
Fracture Width	0.34 in	0.34 in
Total Injection Volume	300,000 gal	
Fluid Efficiency	60%	

During the PEBI mesh process and calculation of cell properties, water saturation is set high in the fractures. Two sets of relative permeability curves are used for the base case, with no surfactant present. Fractures have straight lines for relative permeability curves, while the matrix uses the curves from the history match of lab data. For the SASI case, three sets of relative permeability curves are used for simulation because we separate the matrix into two parts. The matrix region close to the fractures is defined as an invaded zone, where wettability is altered by surfactants. The relative permeability curve for the matrix outside the invaded zone is same as the base case. Due to the limitation of the simulator, the dynamic process of surfactants interacting with rock surfaces and hydrocarbons are not modeled. Alternatively, the final status of the interaction is specified in the simulation as wettability alteration and represented as an immediate switch of relative permeability curves and capillary pressure in the invaded zone. The reservoir model and its properties are shown in Fig. 2. The permeability of the fracture network is set as uniform, although the proppant distribution is non-uniform due to the settling effect (Kou et al. 2018).

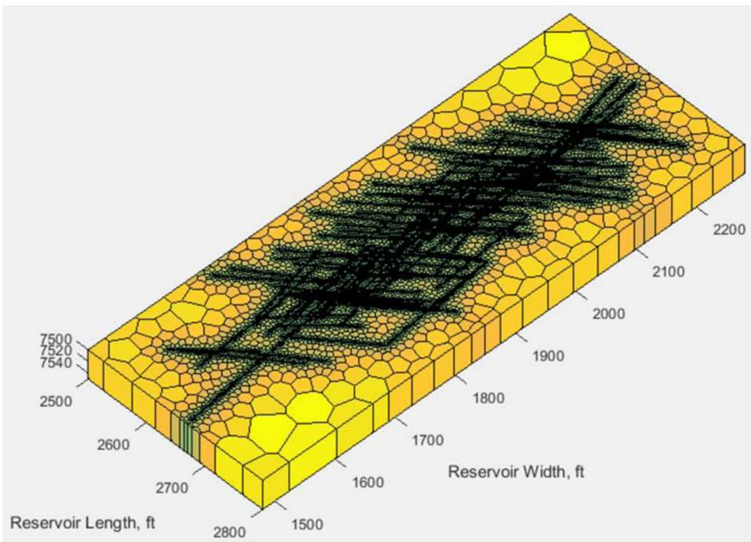

Parameters	Value
Fracture Width (in)	0.34
Fracture Porosity (1)	0.2
Fracture Permeability (mD)	10
Initial Reservoir Pressure (psi)	9000
Reference Pressure (psi)	9000
Reference Datum Depth (ft)	11600
Reservoir Thickness (ft)	50
Reservoir Length (ft)	800
Reservoir Width (ft)	300
Reservoir Top Depth (ft)	11600
Rock Compressibility (1/psi)	5E-08
Horizontal Matrix Permeability (nd)	217
Vertical Matrix Permeability (nd)	217
Matrix Porosity (1)	0.0867
Matrix Water Saturation (1)	0.15
Fracture Water Saturation (1)	0.99
Wellbore Radius (ft)	0.328

Figure 2—2.5D unstructured mesh and properties of the reservoir. The fractures explicitly modeled considered to have a fairly large aperture.

Fluid flow simulation is run for a duration of three years for all the cases. The first 10 days are soak time with the well the shut-in for the surfactant to alter wettability, resulting in wettability alteration before production. Then the bottom hole pressure (BHP) is set to 4300 psi as the constraint to produce, which is slightly higher than the bubble point pressure of 4277 psi.

Results and Discussion

In this part of the work, results from all the work steps are presented. Measurement results from experimental work include interfacial tension, contact angle, and spontaneous imbibition are presented first. These are followed by the capillary pressure curves generated by the scaling group analysis and also relative permeability curves constructed from the history-matching process of core scale model presented in the previous section. Then the results of upscaling to the field-scale from three different methods, scaling group analysis, dual porosity model, and DFN, are presented. In the end, a comparison of results from all three methods is shown to provide an insight into the strength and weakness of each method.

Experimental Results

Contact angle measurements are performed on the core plug before and after it goes through spontaneous imbibition. As shown in Fig. 3, the initial wettability of all the samples is in the oil-wet region as expected from shale rock samples from liquid-rich reservoirs. After being contacted with surfactant solutions of Surf1 and Surf2, the wettability of the samples shifted to the water-wet region. As mentioned in the previous part of this work, a shift of wettability to the water-wet region results in the change of sign of capillary force from negative to positive. Positive capillary pressure will cause oil in the pore to be displaced by water. The contact angle measurement result indicates that the two surfactant solutions tested possess the ability of a wettability altering agent, consequently should also possess the ability to improve oil recovery during spontaneous imbibition.

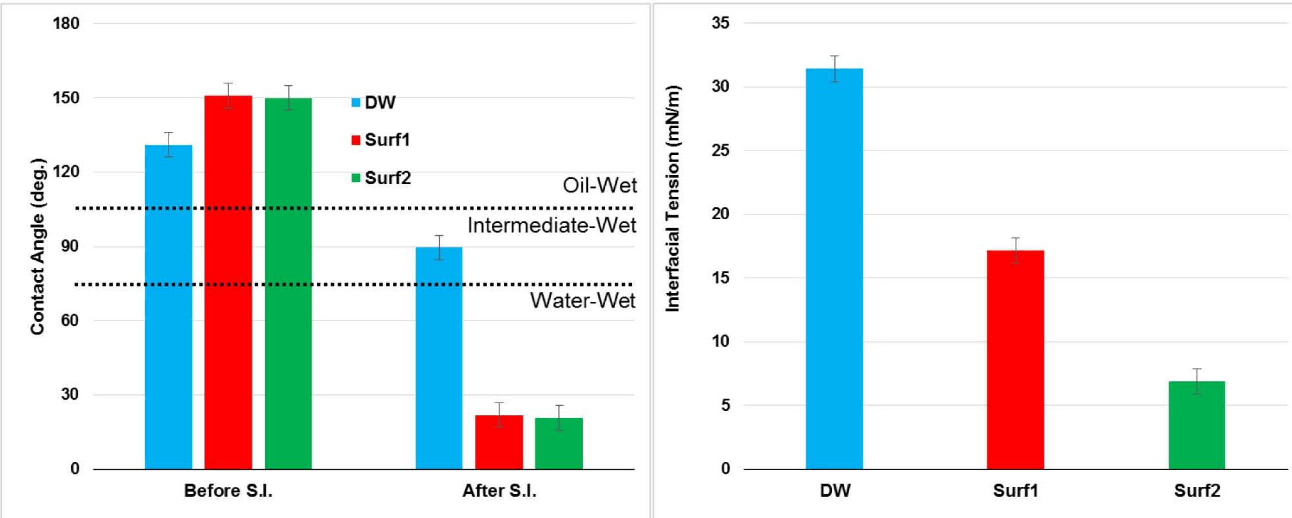

Figure 3—Contact angle results of core plug before and after undergone spontaneous imbibition.

It can be seen that the two surfactant solutions alter the wettability to a similar contact angle value, showing that the wettability alteration effect of the surfactant is identical. However, as indicated by the result of interfacial tension measurement shown in Fig. 3, the two surfactants reduce IFT to different values where Surf2 reduces IFT to 6.9 mN/m compared to 17.14 mN/m of Surf1.The different IFT of the two surfactant solutions is important to observe as IFT controls the magnitude of the capillary driving force. A higher IFT would mean a higher capillary force, which could cause more oil to be produced during the imbibition process. However, lower IFT could also lead to a stronger oil and water fluid exchange because of decreased resistance to the flow of the two fluids. Therefore, higher or lower IFT does not directly translate to better oil production in the imbibition process.

Spontaneous imbibition experiment was run for ten days and the oil production with time lapse of all the three fluid systems can be seen in Fig. 4. Consistent with the previous study on the SASI, the addition of surfactant increases oil recovery compared to a fluid system of water without the presence of a surfactant. A base case for DW shows an ultimate recovery of oil close to the 5% of the original oil in place. Both surfactants increase the recovery factor to more than triple the original recovery as Surf1 produces 18% of the OOIP and Surf2 produces 14% of OOIP. It is also important to notice that in addition to the higher volume of oil recovered from the core plug submerged in the surfactant solution, faster oil recovery is also another advantage of the surfactant-assisted spontaneous imbibition -- oil production reaches a plateau in earlier time on core plugs submerged in surfactant solution compared to the one submerged in water.

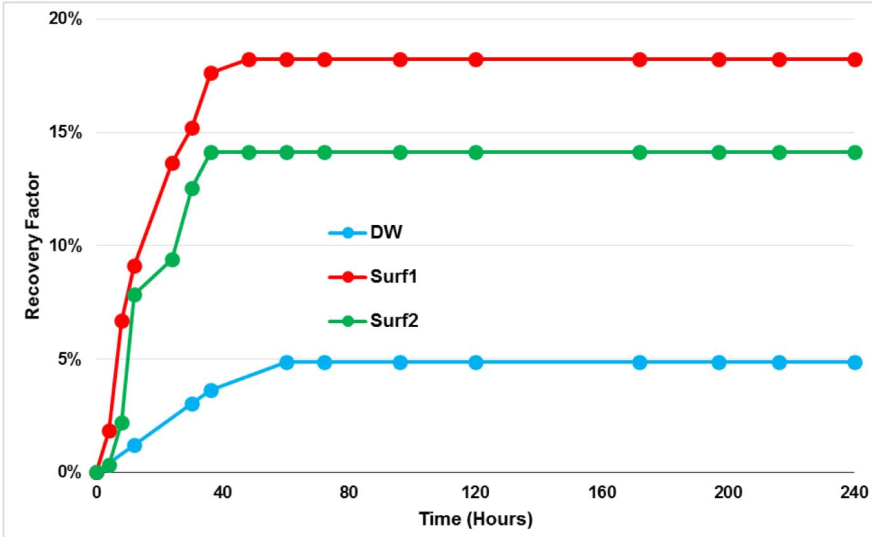

Figure 4—Oil production in time of the spontaneous imbibition experiment.

Capillary Pressure Obtained from Scaling Group Analysis

In order to history match the results of the spontaneous imbibition experiments and upscale the laboratory results to the field through dual porosity model and DFN model, the capillary pressure profiles from each fluid system are required as the input for the simulators. By using the new scaling group that is defined in Eq. 7 to analyze the spontaneous imbibition experiment results, the values of ΔP_cT for each time interval used in the experiments can be calculated, and then used to obtain the ΔP_c values using Eq. 8. We defined capillary pressure (P_c) is equal to zero at ultimate oil recovery due to the fact that spontaneous imbibition ceases when the driving capillary force is equal to zero. By considering initial water saturation, boundary condition, ΔP_c values, and the recovery factors recorded from experiments, we can generate the capillary pressure curves for spontaneous imbibition experiments, as shown in Fig. 5.

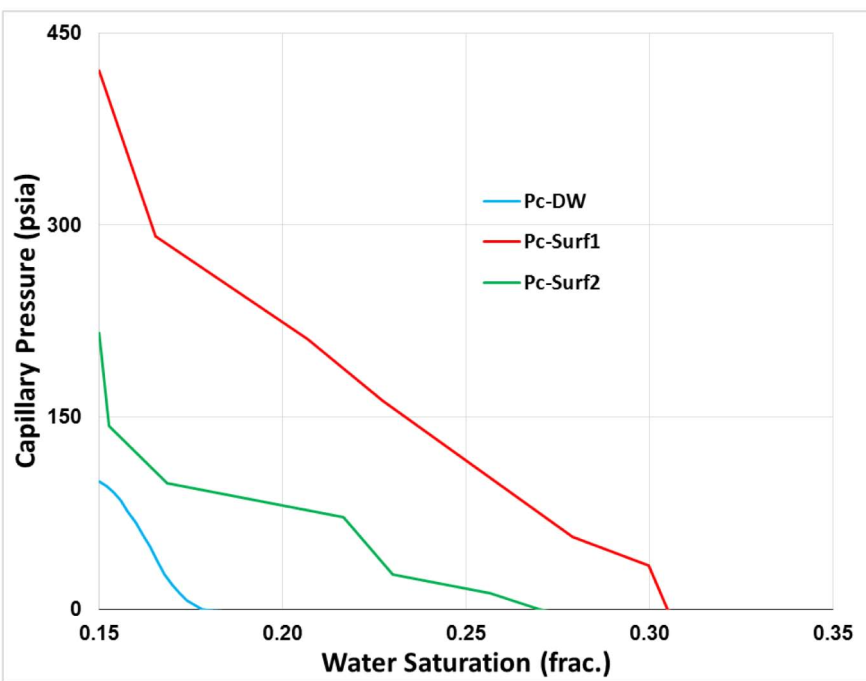

Figure 5—Capillary pressure curves of all three fluid systems as obtained from scaling analysis.

As shown in Fig. 5, the water saturation range starts at initial water saturation which is 0.15 in this case and ends at initial water saturation + ultimate oil recovery. Surf1 has a larger maximum capillary pressure value than Surf2, which is similar to the values obtained from the use CA and IFT measured in the lab to calculate capillary pressure by Young-Laplace equation. In addition, the trend of capillary pressure curves obtained by scaling group analysis is similar to capillary pressure curves generated by existing models.

Relative Permeability Obtained from History-Match on Core-Scale Numerical Model

The digital core model is constructed from the CT-Scan result with the comparison of 3D reconstruction from CT-Scan and grid model used in the simulation can be seen in Fig. 6. With the objective of the rock digitalization using CT-Scan data thus enabling the incorporation of sample heterogeneity into the numerical simulation, the result of the digitalization shows that this objective is achieved as maps of different rock properties seen on the CT images are represented on the rock grid model. It is important to note that the color of CT and grid model is inverted due to the difference in data type shown in the two images. CT images are a map of density and grid models shown in Fig. 6 are maps of porosity. Since density and porosity are inversely related, darker color on CT image will be reflected as brighter color in the grid model, and brighter color on CT image will be shown as darker color on the grid model.

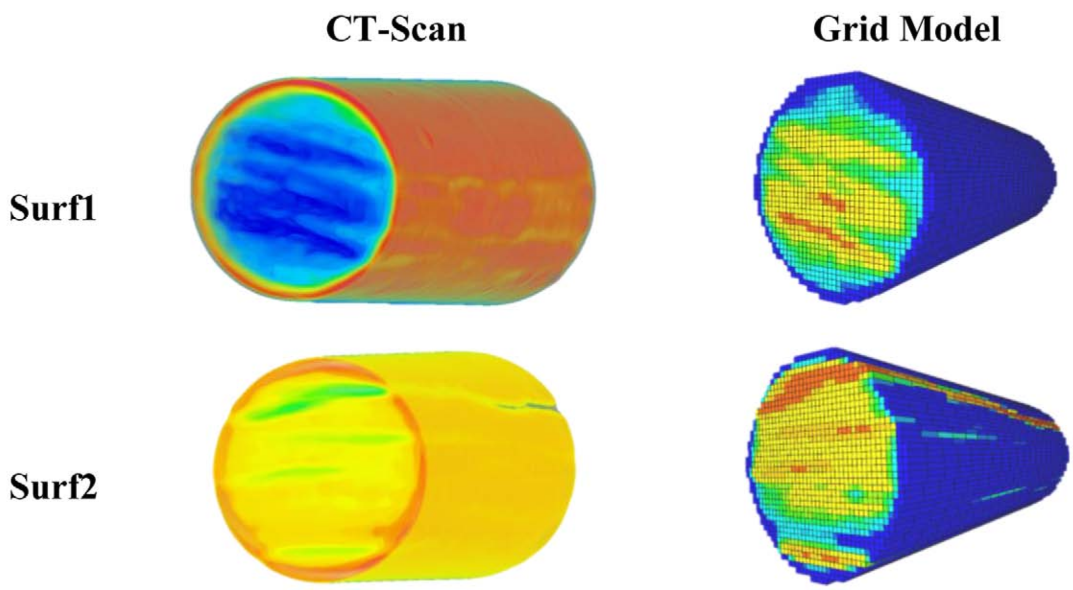

Figure 6—Comparison of CT-Scan 3D reconstruction and grid models of core plugs.

By applying capillary pressure obtained from the scaling group analysis, relative permeability curves are obtained by running history-matching of simulation result to the experimental result. The relative permeability curves plugged into the simulation are all manually constructed by considering the IFT and contact angle values measured in the lab. History-matching requires multiple trial and errors process to be done until the best possible match is achieved. The comparison of simulation and experimental result of spontaneous imbibition experiment is shown in Fig. 7. As can be seen, modeling and experimental results are in good agreement to one another.

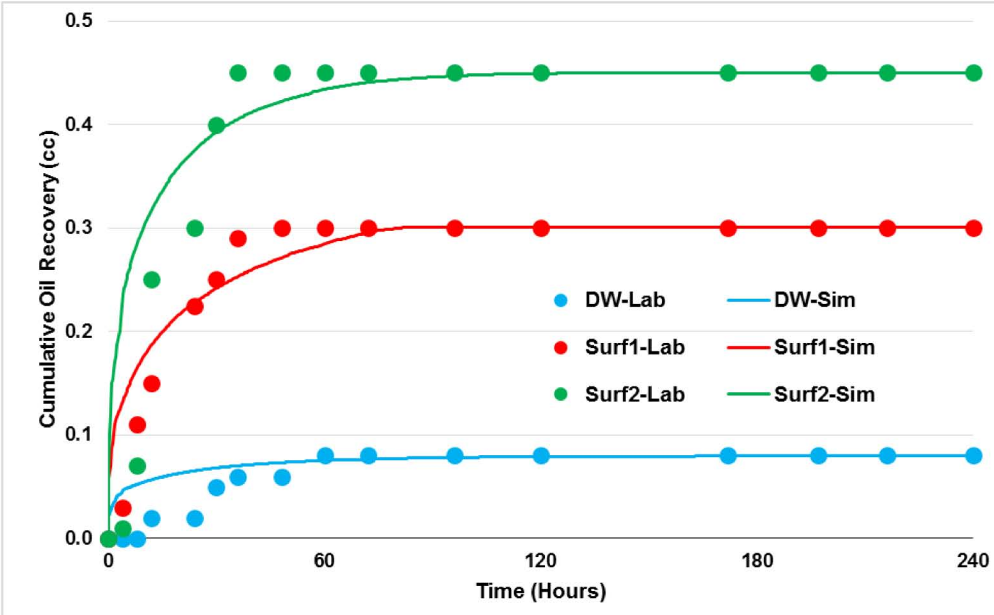

Figure 7—The best history-match result of all three fluid system compared to the experimental data.

Relative permeability curves that provide a match to the recovery curves shown in Fig. 7 is observed in Fig. 8. Comparing the obtained curves to the IFT and contact angle values measured in the lab, several observations can be made. Oil relative permeability curve of Surf2 is higher than that of Surf1 and also DW, which could be related to the lowest IFT value observed on Surf2 followed by Surf1 and DW. Lower IFT would mean easier flow of fluid when the two phases, aqueous and oleic-phase, are present in the pore space, hence resulting in relative permeability curves that are greater. Another cause could be attributed to this observation: as the wettability state of Surf1 and Surf2 is more water-wet compared to DW. Oil will flow easier compared to water with the two surfactant cases when compared to the base case. However, the oil relative permeability of Surf1 and Surf2 are widely separated when compared to the contact angle measurement results of the two. The effect of IFT described before can be used to explain this observation. On the other hand, water relative permeability of water is observed to be the highest, followed by Surf2 then Surf1. The same explanation as before can be applied to explain the observation. Water relative permeability for DW is higher than that for the surfactant system as the wettability state of DW fluid system tends to oil-wet, thus allowing water to flow easier with less attraction from the rock. Water relative permeability of Surf2 is higher than Surf1 due to the lower IFT as measured in the lab.

The wettability state of an oil-water-rock system can be determined by observing the position of the intersection between water relative permeability and oil relative permeability. When the intersection occurs in the area at the right side of 0.5 water saturation line, the wettability of the rock is considered to be water-wet. Conversely, intersection relative permeability curves that intersect to the left side of the mid-point indicates an oil-wet system. By observing the relative permeability curves in Fig. 8, we can see that the intersection point for DW is to the left of 0.5 on the abscissa, indicating oil wettability. This qualitative observation agrees with the contact angle measurements. Intersection points for Surf1 and Surf2 are observed to be on the right side of 0.5 on the abscissa, indicating water-wet behavior, which is also in accordance to the wettability observed from the contact angle measurement.

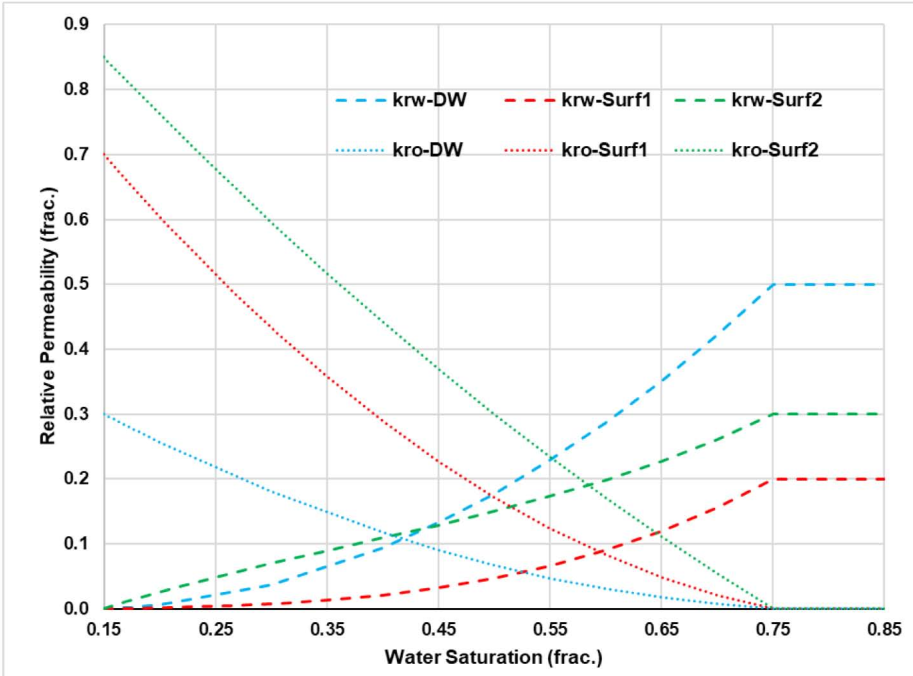

Figure 8—Relative permeability curves as obtained from the history-match process.

Upscaling Laboratory Data to Field-Scale by Dual Porosity Numerical Model

Summary of reservoir properties applied to the dual porosity field-scale model and a screenshot of the grid model can be seen in Fig. 1. Capillary pressure and relative permeability curves of each fluid system are then applied separately into three different cases to observe the effect of SASI on the field-scale to the oil production rate and cumulative oil recovery. Although the model run in the study is a one stage hydraulic fracture model, simulation results are multiplied by 20 to bring the result to realistic well dimension, assuming 20-stage completion is done on the well.

Oil rate and cumulative oil recovery of the dual porosity field-scale model can be seen in Fig. 9. The result indicates that SASI improves both rate and recovery of oil compared to the base case of water without surfactant solution. An increase of 39% to the initial peak oil rate and also 23% increase of 3-year cumulative oil recovery is observed in both cases. A more detail analysis of the curve shows that Surf1 has a slightly higher initial peak oil rate, while Surf2 gives out higher cumulative recovery compared to Surf1. The evidence continues to favor the design of surfactant systems specific to the rock and fluids of interest.

Similar production improvement of Surf1 and Surf2 on the dual porosity field-scale model means a disagreement with the laboratory experiment of spontaneous imbibition, where Surf1 shows a higher recovery compared to Surf2 as illustrated in Fig. 9. In addition, this also contradicts the result of the capillary pressure curve that is obtained analytically, where Surf1 should perform better since capillary pressure curve of Surf1 is higher than Surf2. This discrepancy can be explained by the difference in production mechanism between the field-scale model and the lab-scale model. As explained previously, spontaneous imbibition experiments performed in the lab relies solely on the capillary action of the aqueous phase produce oil. Thus there is no viscous force or pressure difference applied to the rock sample. While at the field-scale, a pressure drawdown is applied to the wellbore in order for the well to be produced. Therefore, in addition to capillary action, viscous forces also affect oil production. Relative permeability of Surf2 is in some sense better than Surf1 as shown in Fig. 8. Viscous displacement as occurred due to the pressure difference is highly dependent on the relative permeability property. Therefore, although Surf1 has a higher capillary curve, we postulate similar performance is observed between Surf1 and Surf2 due to the fact that on the field case both relative permeability and capillary pressure plays a significant role on the performance of the well.

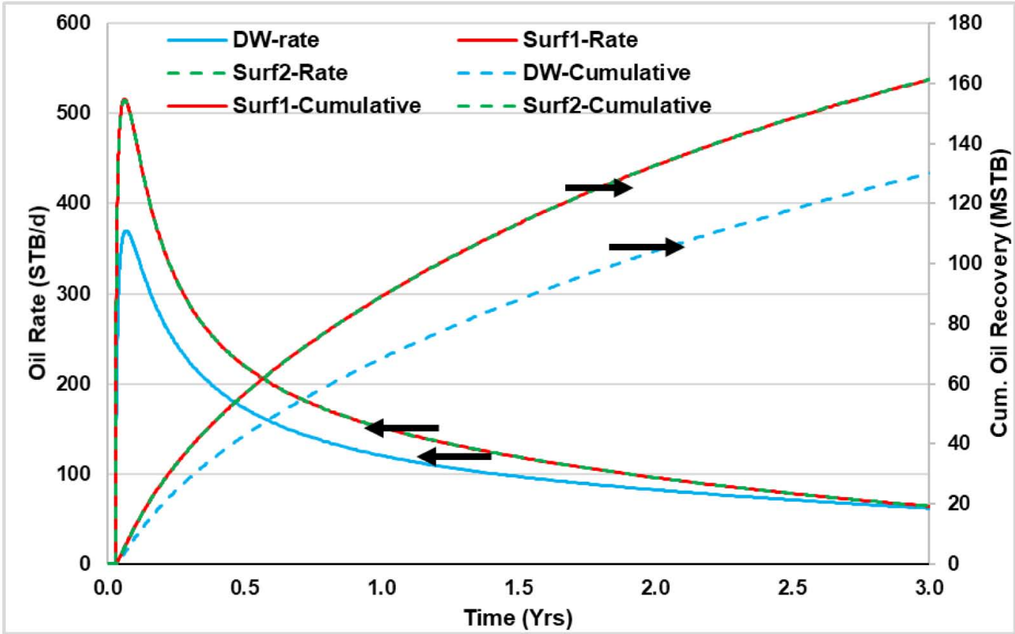

Figure 9—Oil rate and cumulative recovery comparison of dual porosity field-scale model.

Upscaling Laboratory Data to Field-Scale by Analytical Method

In this section, we utilize the spontaneous imbibition experimental results which have been presented in this paper in order to scale laboratory data to the field. By considering oil recovery data recorded during the spontaneous imbibition experiments and Eq. 13-14, the production rate curves and normalized production rate curves for all three cores can be plotted in Fig. 10. Due to the assumption that the value of dimensionless time for spontaneous imbibition experiment and the field case is constant, the predicted field normalized production rate curve has the same shape as a normalized production curve obtained from laboratory data.

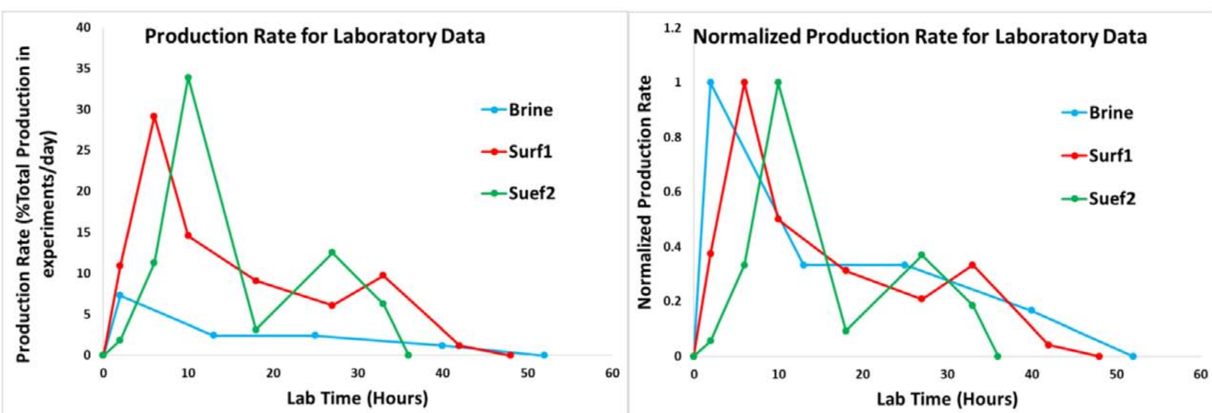

Figure 10—Calculated production rate from cores during spontaneous imbibition experiments.

Fig. 10 demonstrates that the values of production rate for spontaneous imbibition experiments reach a maximum within 12 hours. Due to the effectiveness of the surfactant in wettability alteration and IFT reduction, experiments have different imbibition rates that lead to maximum production rates occurring at different times. For the brine case without surfactant, water cannot effectively penetrate into the core due to the absence of water-wet surface. Therefore the production rate for brine is much less than all other cases. The normalized production rate curves indicate that spontaneous imbibition can be separated into three parts: high production during the initial phase, stable production followed by a steady but low production phase.

For the high production phase, the surfactant solution is efficiently imbibed into the core, and consequently oil is recovered due to a change in wettability from oil wet to water wet as well as a simultaneous decrease in IFT. After wettability alteration and IFT reduction in the core sample, spontaneous imbibition experiments enter a stable phase where the production rate maintains around 30-40% of maximum values, due to relative permeability and capillary pressure that is decreasing as the water saturation increases. During the low production phase, the production rate decreases to zero due to the size of the core samples and the finite volume of oil in these small pore spaces.

As shown in Fig. 10, the cumulative oil production for brine, Surf1 and Surf2 experiments reach half of the total oil production at 20 hours, 12 hours and 11 hours, respectively. Based on the IHS Energy Database, we analyzed the production date of the reservoir where the sidewall cores and oil samples were collected. Typically, half of the cumulative oil production for a well in unconventional reservoirs is usually produced within the first year. By considering the dimensions of the cores, laboratory time and field time, the characteristic lengths of the core samples and field can be estimated by using Eq.10 and Eq. 11, which is presented in Table 2.

Table 2—Core characteristic length

Core	Type of Fluid	$L_{c(Lab)}$ (cm)	$L_{c(filed)}$ (cm)
1	DW	0.86	56.2
2	Surf1	0.77	71.3
3	Surf 2	0.85	83.2

In order to scale the laboratory data to the field, we assume that the induced open fracture layout is shown in Fig. 11. The total fracture area for the fracture distribution as seen in Fig. 11 is equal to 7 times the hydraulic fracture area. For both sides of the primary hydraulic fracture, the induced fracture creates one layer of equal-size cubic matrix blocks that close to hydraulic fracture. The imbibition in the field scale can be described as spontaneous imbibition for these equal-size cubic blocks surrounded by aqueous solution, which is similar to imbibition experiments in the lab. The side length of these cubic blocks can be calculated from the characteristic length of the field, which is used to estimate the cumulative oil production from imbibition in the field, and then used to predict the field production rate for imbibition.

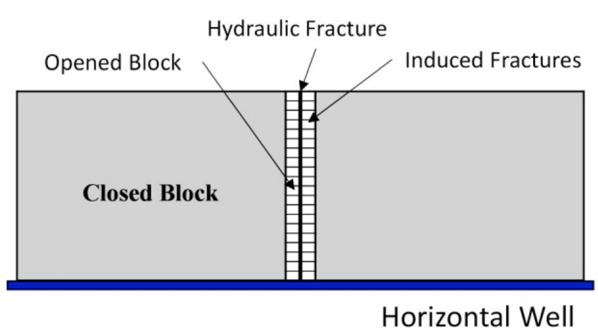

Figure 11—Induced and hydraulic fractures layout along the horizontal well.

Since the purpose of this study is to compare upscaling results for one analytical and two numerical models, we defined a constant total fracture volume for all three models, which is 300,000 gal/stage. In this paper, we assume the average width of open fractures is about 0.02 ft. By considering the fractures distribution shown in Fig. 11, total fracture volume, fracture width, and the area of hydraulic fracture can be calculated by Eq. 15, where V_f fracture volume, and w is average fracture aperture. The cumulative oil production in the field by imbibition can be calculated by Eq.12, which is presented in Table 3. Coupled with normalized production curves obtained from experimental data, we plot the predicted field oil production rate and cumulative oil production curves for one stage in Fig. 12.

$$A = \frac{V_f}{7w} \tag{15}$$

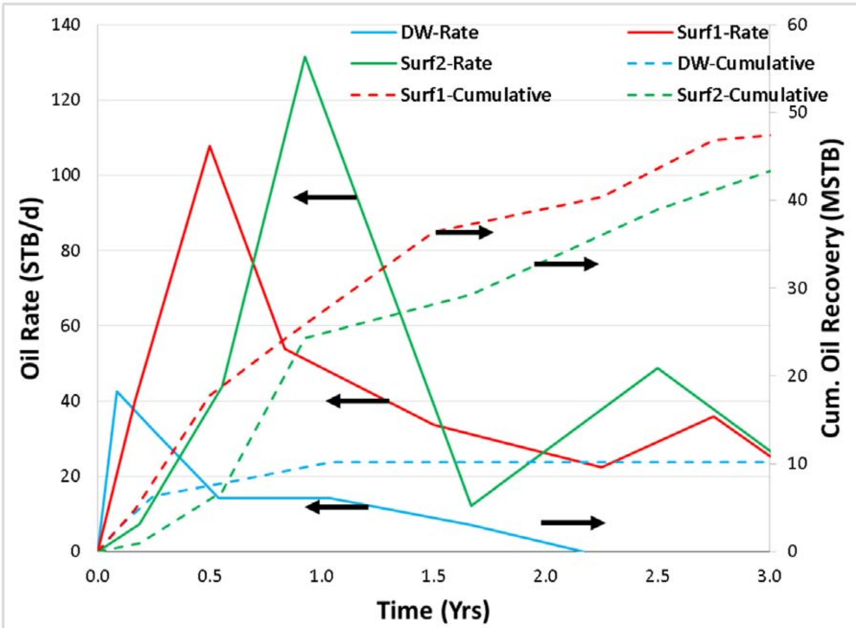

Figure 12—Oil rate and cumulative recovery for imbibition up-scaled by analytical.

As shown in Fig. 12, the Surf1 reaches maximum oil production rate faster than Surf2 due to greater capillary pressure after wettability alteration and IFT reduction. Another interesting observation observed in Fig. 12 is that although Surf2 has a higher peak oil production rate compared to Surf1, cumulative oil recovery of Surf1 is higher than that of Surf2, similar to the laboratory data. Based on the upscaling results, the field production rates for imbibition increases when the surfactant is added to the completion fluid. Compared with the base case, oil production rates increases by 2 to 5 bbl/day per stage (40 to 100 bbl/day for the whole well) due to wettability alteration and IFT reduction, which can be used to prove the effectiveness of surfactants on enhancing oil recovery in ULR. In addition, the predicted cumulative oil production for imbibition increases as the total area of open fractures is increased according to Eq.12, since the aqueous solution has a more extensive contact or surface area that naturally results in more oil extraction by imbibition.

Table 3—Cumulative oil production for one stage in the field by imbibition

Type of Fluid	DW	Surf1	Surf2
Cumulative Oil Production (bbl)	509.85	2424.18	2191.78

The total production of a well consists of the oil produced by the pressure difference between the reservoir and the wellbore including imbibition. The oil production driven by pressure difference contributes to a significant proportion for the production of a well. Therefore, the total production rates are the sum of the drawdown plus the additional oil recovered by SASI in each case. Observation of simulation results of the DW case which presumably is due primarily to drawdown, observation of the imbibition oil produced is the difference between the Surf1 and Surf2 curves minus the cumulative production DW with no SASI as shown in Fig. 13.

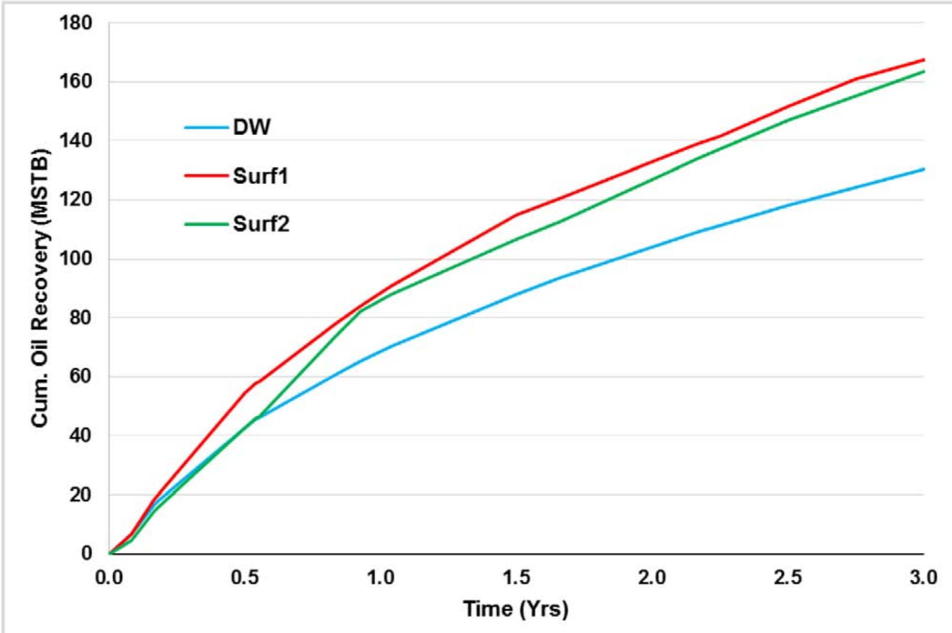

Figure 13—Oil rate and cumulative recovery upscaled by analytical.

Upscaling Laboratory Data to Field-Scale by Discrete Fracture Network Model

The simulation results of the DW base case and surfactant soaking cases from DFN models are shown in Fig. 14. For each surfactant, the effect of the invaded zones is assumed to be 2 ft, 20 ft around fractures, and in addition to the assumption that the entire reservoir has some penetration by imbibition. Fig. 14 demonstrates that the production is enhanced if the surfactants are added. And the effect of the enhanced recovery is reinforced with an increase of invaded area. In addition, at the very beginning, sharp peaks exist for the surfactant cases, especially for the cases of the fully invaded reservoir. Such peaks result from the matrix oil exchanged to the fracture from the matrix, driven by the capillary pressure during the soaking period (Fig. 15). After the peak, the relatively high oil saturation in the fractures also helps maintain a high in-situ effective oil permeability. Additionally, compared to the uninvaded zone, higher effective oil permeability covering all saturations in the invaded zone, where wettability alternates, also contribute to the oil production increases. These concepts of depth of penetration need further study to determine the contribution of imbibition and relative permeability change at different production periods. Moreover, the area of invaded zone is also highly uncertain.

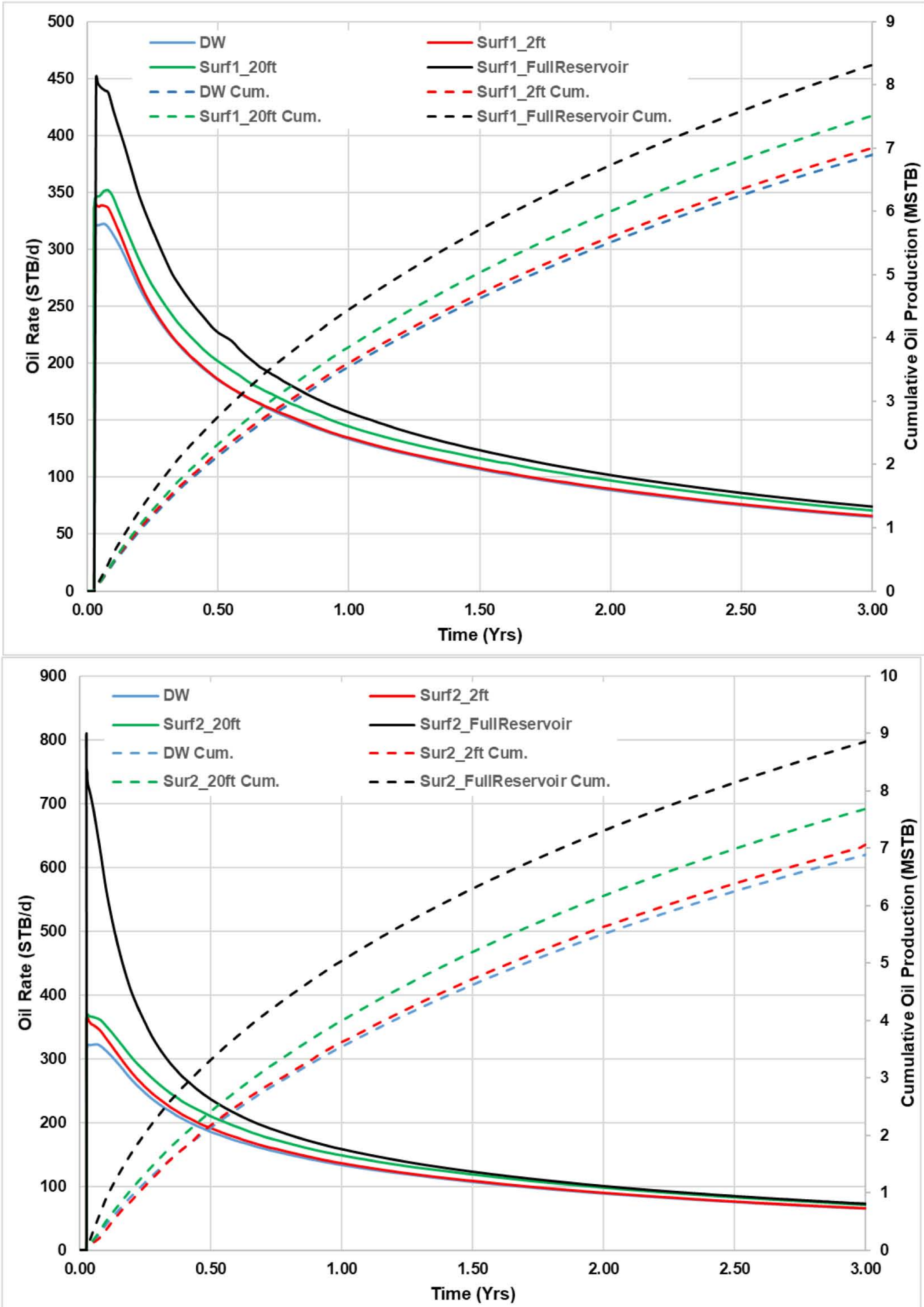

Figure 14—3-year oil production rates and cumulative oil production from the cases of two kinds of surfactant fluids with various invaded distance (2ft, 20 ft, and full reservoir), compared to the rates from DW base case.

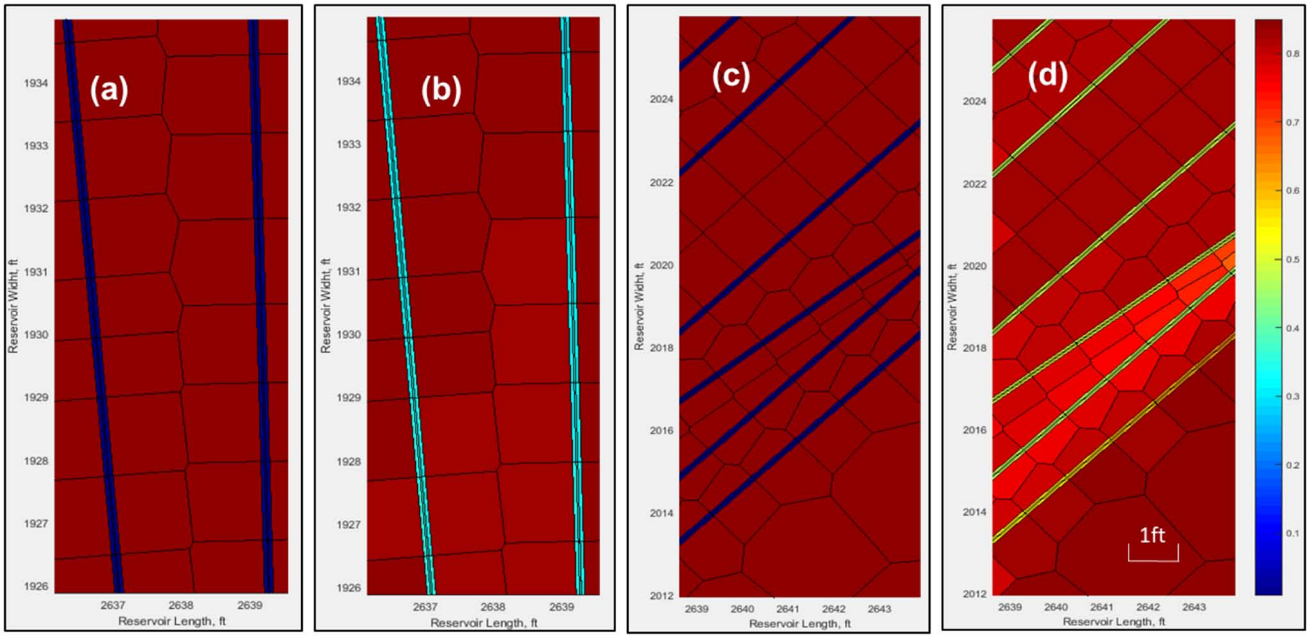

Figure 15—Oil Saturation at the beginning (a)(c) of soaking (day 1) and the end (b)(d) of soaking (day 10). (a)(b) are from Surf2_2ft, while (c)(d) is from Surf2_FullReservoir. The oil saturation in fractures increases from 0.01 to about 0.35 and 0.55 respectively for the two cases after soaking.

Comparison of Analytical, Dual Porosity Model, and Discrete Fracture Network Upscaling Method

The comparison of the three methods to forecast the oil recovery enhancement by surfactant at field scale is shown in Fig. 16.

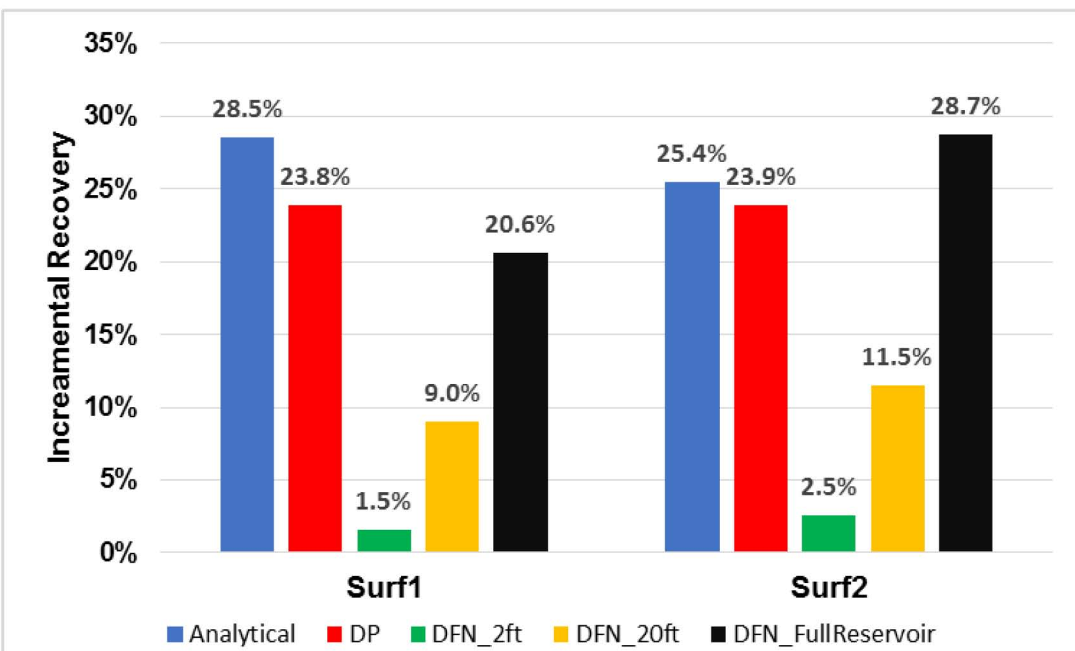

Figure 16—Incremental recovery obtained from three methods.

The dual porosity model has large incremental recovery over 20%, which assumes all fractures surround matrix blocks at some fracture spacing thus a guarantee that the entire reservoir matrix is invaded. The upscaling results of the analytical method show the additional recovery by surfactant additives is over 25% and Surf1 has a better performance than that of Surf2 in the field because this method only considers the effect of spontaneous imbibition driven by the capillary pressure and Surf1 has a higher capillary force. But the oil relative permeability affected by Surf1 is lower than that affected by Surf2, which is not taken into consideration in the analytical method. The dual porosity method shows a similar incremental recovery for the two surfactants, which is a result of dynamic effects of surfactant adsorption, capillary pressure, and relative permeability alteration. However, the DFN method includes the effects of capillary pressure and relative permeability change, but the wettability alteration and IFT reduction are completed immediately in this DFN study due to the lack of capability of the simulator to model surfactant dynamic behavior. On the other hand, we investigated three cases for our DFN model due to the fact that the extent of the region affected by surfactant is uncertain. In the case where the whole reservoir is invaded, maximum incremental oil recovery by surfactant addition is observed. However, this maximum value is a highly-optimistic case due to the small possibility of the wettability of the entire well volume being altered by the surfactant. By considering microfractures and leak off effects, the incremental oil recovery should be more significant than the 2-ft invade zone case. Therefore, the argument can be made that penetration is greater than we may believe resulting in an additional recovery by surfactant additives more similar to the 20-ft invaded zone case.

Summary

In summary, the results of experiments indicate that the wettability alteration and IFT reduction play a significant role in improving oil recovery in the unconventional liquid reservoirs. We defined a new scaling group to deal with capillary pressure curves for spontaneous imbibition. By considering capillary pressure profiles and history matching of laboratory data with numerical simulation, the relative permeability curves can be generated, and imported to dual porosity models and DFN models to predict production data in the field. This study proposes three methods to upscale laboratory results to the field based on analytical analysis and numerical simulation.

The spontaneous imbibition experiment results indicate that the ultimate oil recovery factor by using Surf1 is 29.1% higher than the Surf 2. However, the upscaling result shows that the cumulative oil production for imbibition of the Surf1 case is 12.5% greater than the Surf2 case by the analytical method. In addition, for both dual porosity models and DFN models, the Surf2 has a better performance than Surf1 in the field simulation. The imbibition rate and the relative permeability of Surf2 are larger than Surf1, which could lead to better performance of Surf2 in the field. Further study regarding this finding on the imbibition rate and model improvement will be performed in the future to establish how the actual surfactant groups can be optimized and/or designed.

Our analysis indicates that all of these methods can be used to predict incremental production by adding surfactants with the completion fluid. The estimated production rate and cumulative oil production for the field by the scaling group analysis methods are comparable to numerical simulation results, which can be used to validate the analytical model. The effectiveness of surfactants for wettability and IFT alteration as well as the surface area of open fractures determines incremental oil recovery in the field from imbibition. The upscaling results of scaling group analysis method show that 3-year cumulative oil production increases 28.5%. The analytical method achieves the highest oil recovery incremental than other two simulation methods due to the neglect of the relative permeability effect. But the upscaling results by the analytical approach are still in the reasonable region. We can use this method to obtain an accurate approximation without the need of massive computational power required by the numerical methods. The simulation results of the dual porosity model on the field show that the initial peak oil production rate increases 39% and the 3-year cumulative oil production increases 23%. For DFN model, the simulation results indicate that the cumulative oil production increases in a range of 1.52% to 28.7% based on the type of surfactants and extent of the invaded area. The upscaling results show that the oil production can be enhanced by surfactant-assisted spontaneous imbibition, which is similar as observed in the laboratory experiments.

Conclusions

1. Surfactant additives in stimulation fluids can alter the wettability of a given rock surface and decrease IFT, which can be used to improve oil recovery in unconventional liquid reservoirs.
2. A scaling group is developed to generate capillary pressure profiles for spontaneous imbibition experiments. The generated capillary pressure curves from scaling group analysis are validated by history match to the laboratory results.
3. Upscaling laboratory results of spontaneous imbibition experiments to the field through scaling group analysis provides a fast and reasonable method to predict oil recovery incremental from surfactant-assisted imbibition in ULR.
4. Numerical simulation performed with dual porosity field-scale models indicates that production performance enhancement by SASI as observed in laboratory experiments also works at the field-scale. Initial peak oil rate increases of 39% and 3-year cumulative oil recovery increase of 23% are achieved in the field simulation.
5. Simulation with DFN shows the oil recovery of a fractured reservoir could be increased by surfactant, ranging from 1.52% to 28.70%, depending on the type of surfactant and the extent of the invaded area.
6. All three methods can be used to upscale laboratory results to predict field performance, although the physical models of each method differ significantly. Further study is needed to improve the accuracy of these methods.

Acknowledgements
The authors would like to thank Crisman Institute for Petroleum Research at Texas A&M University for funding this work. We also would like to thank the staff and student workers at the Department of Petroleum Engineering in Texas A& M University for their collaboration on the experimental work.

Nomenclature

A = Area of the open fracture surface
c = Constant value in Eq. 3
d = Diameter of core samples
l = Length of core samples
l_d = Distance of water penetrates into the reservoir matrix
L_c = Characteristic length
k = Permeability
k_{re}^* = The relative permeability pseudo-function of the two phases
P_c = Capillary pressure
ΔP_c = Capillary pressure difference
$\Delta P_c\mathrm{T}$ = Defined parameter for capillary pressure multiplied by time
q = Production rate
q_n = Normalized production rate
R = Pore radius
S_o = Oil saturation
S_{wf} = Water saturation
S_{wi} = Initial water saturation
t = Laboratory time
$t(field)$ = Field time
$\mathrm{t_{mid}}$ = Mean time between two recorded times
t_D = Dimensionless time for laboratory scale

$t_{D(field)}$ = Dimensionless time in the field
θ = Contact angle
μ_e = Effective viscosity of the two phases
μ_o = Oil viscosity
μ_w = Water viscosity
σ = Interfacial tension (IFT)
ϕ = Porosity

References

Adel, I.A., Fan, Z., Bhatnagar, N. et al. 2018. The Impact of Gas-Assisted Gravity Drainage on Operating Pressure in a Miscible CO2 Flood. Presented at the SPE Improved Oil Recovery Conference, Tulsa, Oklahoma, USA. https://doi.org/10.2118/190183-MS.

Adel, I.A., Tovar, F.D., and Schechter, D.S. 2016. Fast-Slim Tube: A Reliable and Rapid Technique for the Laboratory Determination of MMP in CO2 - Light Crude Oil Systems. Presented at the SPE Improved Oil Recovery Conference, Tulsa, Oklahoma, USA. https://doi.org/10.2118/179673-MS.

Alvarez, J.O., Neog, A., Jais, A. et al. 2014. Impact of Surfactants for Wettability Alteration in Stimulation Fluids and the Potential for Surfactant EOR in Unconventional Liquid Reservoirs. Presented at the SPE Unconventional Resources Conference, 1-3 April, The Woodlands, Texas, USA. https://doi.org/10.2118/169001-MS.

Alvarez, J.O., Saputra, I.W.R., and Schechter, D.S. 2017. The Impact of Surfactant Imbibition and Adsorption for Improving Oil Recovery in the Wolfcamp and Eagle Ford Reservoirs. Presented at the SPE Annual Technical Conference and Exhibition, 9-11 October, San Antonio, Texas, USA. https://doi.org/10.2118/187176-MS.

Alvarez, J.O., Saputra, I.W.R., and Schechter, D.S. 2017. Potential of Improving Oil Recovery with Surfactant Additives to Completion Fluids for the Bakken. *Energy & Fuels* **31** (6): 5982-5994. https://doi.org/10.1021/acs.energyfuels.7b00573.

Alvarez, J.O. and Schechter, D.S. 2015. Wettability Alteration and Spontaneous Imbibition in Unconventional Liquid Reservoirs by Surfactant Additives. Presented at the SPE Latin American and Caribbean Petroleum Engineering Conference, 18-20 November, Quito, Ecuador. https://doi.org/10.2118/177057-MS.

Alvarez, J.O. and Schechter, D.S. 2017. Wettability Alteration and Spontaneous Imbibition in Unconventional Liquid Reservoirs by Surfactant Additives. *SPE Reservoir Evaluation & Engineering*. SPE-177057-PA. https://doi.org/10.2118/177057-PA.

Du, S., Liang, B., and Yuanbo, L. 2017. Field Study: Embedded Discrete Fracture Modeling with Artificial Intelligence in Permian Basin for Shale Formation. Presented at the SPE Annual Technical Conference and Exhibition, 9-11 October, San Antonio, Texas, USA. https://doi.org/10.2118/187202-MS.

Fischer, H., Wo, S., and Morrow, N.R. 2008. Modeling the Effect of Viscosity Ratio on Spontaneous Imbibition. *SPE Reservoir Evaluation & Engineering* **11** (03): 577-589. SPE-102641-PA. https://doi.org/10.2118/102641-PA.

Gupta, A. and Civan, F. 1994. An Improved Model for Laboratory Measurement of Matrix to Fracture Transfer Function Parameters in Immiscible Displacement. Presented at the SPE Annual Technical Conference and Exhibition, 25-28 September, New Orleans, Louisiana. https://doi.org/10.2118/28929-MS.

Kou, R., Moridis, G.J., and Blasingame, T.A. 2018. Analysis and Modeling of Proppant Transport in Inclined Hydraulic Fractures. Presented at the SPE Hydraulic Fracturing Technology Conference and Exhibition, 23-25 January, The Woodlands, Texas, USA. https://doi.org/10.2118/189856-MS.

Leverett, M.C. 1939. Flow of Oil-Water Mixtures through Unconsolidated Sands. *Transactions of the AIME*. SPE-939149-G. https://doi.org/10.2118/939149-G.

Li, K. and Horne, R.N. 2002. Scaling of Spontaneous Imbibition in Gas-Liquid-Rock Systems. Presented at the SPE/DOE Improved Oil Recovery Symposium, 13-17 April, Tulsa, Oklahoma. https://doi.org/10.2118/75167-MS.

Ma, S., Morrow, N.R., and Zhang, X. 1995. Generalized Scaling of Spontaneous Imbibition Data for Strongly Water-Wet Systems. Presented at the Technical Meeting / Petroleum Conference of The South Saskatchewan Section, October 16 - 18, Regina. https://doi.org/10.2118/95-138.

Mattax, C.C. and Kyte, J.R. 1962. Imbibition Oil Recovery from Fractured, Water-Drive Reservoir. *SPE J* **2** (02): 177-184. SPE-187-PA. https://doi.org/10.2118/187-PA.

Niu, G., Sun, J., Parsegov, S. et al. 2017. Integration of Core Analysis, Pumping Schedule and Microseismicity to Reduce Uncertainties of Production Performance of Complex Fracture Networks for Multi-Stage Hydraulically Fractured Reservoirs. Presented at the SPE Eastern Regional Meeting, 4-6 October, Lexington, Kentucky, USA. https://doi.org/10.2118/187524-MS.

Parsegov, S.G., Niu, G., Schechter, D.S. et al. 2018. Benefits of Engineering Fracture Design. Lessons Learned from Underperformers in the Midland Basin. Presented at the SPE Hydraulic Fracturing Technology Conference and Exhibition, 23-25 January, The Woodlands, Texas, USA. https://doi.org/10.2118/189859-MS.

Sun, J., Niu, G., and Schechter, D. 2016. Numerical Simulation of Stochastically-Generated Complex Fracture Networks by Utilizing Core and Microseismic Data for Hydraulically Fractured Horizontal Wells in Unconventional Reservoirs–a Field Case Study. Presented at the 2016 SPE Eastern Regional Meeting, Canton, Ohio. 13–15 September. https://doi.org/10.2118/184077-MS.

Sun, J. and Schechter, D. 2017. Pressure-Transient Characteristics of Fractured Horizontal Wells in Unconventional Shale Reservoirs with Construction of Data-Constrained Discrete-Fracture Network. *SPE Production & Operations*. SPE-184060-PA. https://doi.org/10.2118/184060-PA.

Sun, J. and Schechter, D.S. 2015. Investigating the Effect of Improved Fracture Conductivity on Production Performance of Hydraulic Fractured Wells through Field Case Studies and Numerical Simulations. *Journal of Canadian Petroleum Technology* **54** (6): 442 - 449. https://doi.org/10.2118/169866-PA.

Wang, D., Zhang, J., Butler, R. et al. 2016. Scaling Laboratory-Data Surfactant-Imbibition Rates to the Field in Fractured-Shale Formations. *SPE Reservoir Evaluation & Engineering*. SPE-178489-PA. https://doi.org/10.2118/178489-PA.